

# Simulating debris flow deposition using a two-dimensional finite model and Soil Conservation Service-curve number approach for Hanlin gully of southern Gansu (China)

Peng Zhang · Jinzhu Ma · Heping Shu ·  
Tuo Han · Yali Zhang

Received: 4 July 2014 / Accepted: 4 November 2014 / Published online: 15 November 2014  
© Springer-Verlag Berlin Heidelberg 2014

**Abstract** Evaluating the flood discharge and deposition process of a debris flow is important for risk assessment, management, and design of possible supporting works for geo-hazard mitigation. The movement and deposition process of a typical debris flow gully in southern Gansu province, China, was simulated using the Soil Conservation Service-curve number (SCS-CN) approach and a two-dimensional finite model (FLO-2D PRO model) coupled with geographic information systems. Runoff volumes and depths were obtained by the use of the SCS-CN model using different precipitations and different intervals. The deposition, velocity, impact force, and influence zone of the debris flow were simulated with the FLO-2D PRO model based on the results of the SCS-CN method. Simulation results for a storm that occurred on 12 October 2010 suggest a maximum flow velocity of 23.1 m/s, a maximum deposition depth of 27.9 m, and a hazard zone of about 0.414 km<sup>2</sup>. These results were consistent with measured results from the documented debris flow. Verification demonstrated that model results could be used to help predict disaster-causing debris flows, thus helping to protect the lives, property, and economy of the local population.

**Keywords** Soil Conservation Service-curve number · FLO-2D · GIS · Debris flow · Hazard zone · Hanlin gully

## Introduction

Debris flows consisting of sediment and water that moves as a continuous fluid driven by gravity are natural geo-hazard phenomena in mountainous regions. A debris flow attains high mobility from an enlarged void space that is saturated with water or slurry as a result of its coupling with topography, geomorphology, geological structure, precipitation, loose debris, vegetation, and human activities (Takahashi 2007). High-velocity debris flows can devastate villages, farmland, and infrastructure, and can move and deposit large amounts of sediment, impacting riverbed evolution over a short time period. Heavy cutting/erosion of upstream channels may lead to landslides and failures in riverbeds. Research into debris flows, using numerical simulation of their movement and deposition processes, can provide important insight for their prevention and mitigation. As a result of rapid socio-economic development, recent patterns and intensity of land use have had a significant effect on runoff yields, playing important roles in the occurrence and development of debris flows in small catchments (Zhang et al. 2014; Dongquan et al. 2009; Turconi et al. 2013).

Debris flows are closely linked to the hydrological processes of watersheds. The Soil Conservation Service-curve number (SCS-CN) method is a popular approach for computing the direct surface runoff from a rainstorm and is widely used to estimate and forecast runoff from small- and medium-sized catchments. The SCS-CN method is simple, stable, and easy to understand and apply, and can implicitly interpret the runoff-generating properties of the catchment (Mishra et al. 2012; Doglioni and Simeone 2014). It incorporates the influence of watershed characteristics, such as soil type, land use, hydrological conditions, and antecedent moisture conditions (AMCs) on rainfall–runoff

---

P. Zhang · J. Ma (✉) · H. Shu · T. Han · Y. Zhang  
Key Laboratory of Western China's Environmental Systems  
(MOE), Lanzhou University, Lanzhou 730000, China  
e-mail: jzma@lzu.edu.cn

(Hadadin 2013). Yu (2012) used rainfall intensity and storm runoff data to test the assumption of proportionality between retention and runoff that underpins the SCS approach. The CN approach was used to generate realistic runoff data by incorporating the revised soil-moisture index method and a macro spreadsheet to forecast the mean annual removal efficiencies of wet detention ponds (Williams et al. 2012; Youn and Pandit 2012). Other researchers have improved the SCS-CN method (Tsai and Wang 2011; Suresh Badu and Mishra 2012; Sahu et al. 2012; Jain et al. 2012). Recently, the SCS-CN approach has been coupled with remote sensing imaging and GIS data to effectively simulate runoff production (Gupta et al. 2012; Nagarajan and Poongothai 2012; Jena et al. 2012).

O'Brien et al. (1993) developed FLO-2D, a two-dimensional finite model that can simulate debris flows and used this model to simulate the 1983 Rudd Creek mudflow event in Utah. The parameters for the FLO-2D model were calibrated and this model was successfully used in the Yosemite Valley, California and in Hualien County, Taiwan, to replicate the hazard zone of a debris flow event (Bertolo and Wiczorek 2005; Hsu et al. 2010). Peng and Lu (2012) used the FLO-2D model to simulate a mudflow resulting from a large landslide caused by extremely heavy rainfall in southeastern Taiwan. FLO-2D was also coupled with the Debris-2D program to demonstrate its effectiveness simulating actual debris flow (Wu et al. 2012). Other studies have suggested that FLO-2D is reasonably well developed and effective for actual case applications (Xu et al. 2014; Aleotti and Polloni 2003; Garcia et al. 2003; Chen et al. 2010; Peng and Lu 2012).

The main objectives of the present study were to (1) use the SCS-CN model to simulate the rainfall–runoff processes of the Hanlin gully in southern Gansu province, (2) simulate the zone of influence and deposition depth of a debris flow that occurred at this location, and (3) compare the simulation results with the zone of influence and deposition depth of an actual debris flow that occurred at this location.

## Study area

The study area, the Hanlin gully, is located in the middle-lower reaches of the Bailong River Basin, which lies at the boundary between the subtropical and warm temperate zones (Zhuang et al. 2013) of western China (Fig. 1). The Bailong River covers an area of approximately  $17.8 \times 10^3$  km<sup>2</sup> in the southern Gansu province and has precipitous terrain, with many crisscrossing ravines and gullies, high mountains, steep slopes, and deep valleys. The mean elevation in the Bailong River Basin ranges from 550 m to 4536 m asl and slopes are generally greater than 30°. The

mean annual air temperatures range from 12 to 14.0 °C, depending on the elevation, solar radiation, topography, and other local factors. The mean annual precipitation ranges from 500 to 900 mm, of which about 60 % of the annual total falls from June to September, mostly in the form of summer rainstorms (Dai and Lee 2001).

The area is controlled by Qinghai–Tibet tectonic belt and Wudu arc structure and is affected by uplift of the Qinghai–Tibet Plateau (Bai et al. 2008), and especially is strongly influenced by neotectonic activity. Large duplex folds structure mainly develops in west Qinling orogenic belt, and the Beiyu duplex anticline is taken as representative. The long-term tectonic activity showed roughly parallel extrusion zone along NW trend in the western and EW trend in the eastern, including folds and faults. The intervening stratum also shows NW–NWW trend as a band. Rock extrusion and fracture folds are common, resulting in broken strata that have been subject to intense weathering processes. Strong seismic activity and high rainfall intensity within the Bailong River Basin are the main reasons for landslides and debris flows (Bai et al. 2008). Soil type is classified according to the Chinese soil taxonomy in the study area (NSSO 1998), and the major types of soil are gravel soil, loam, silty clay, clay, and paddy soil. Water erosion, wind erosion, debris flows, gully erosion, landslides, and slope erosion are the main types of soil erosion in the study area. This area has the most serious debris flows or landslides in southern Gansu province.

The area of the Hanlin gully is 33.98 km<sup>2</sup>; its main channel is 9.45 km long; and the slope of the main channel is 10.6 %. The relative elevation difference in the gully is 1,648 m and the recharge length ratio of sediment along the main channel is 0.65 %. The Hanlin gully has generated frequent, viscous debris flows with an average interval of 10 years. The rock within the gully is completely weathered. After the earthquake that happened on 12 May, 2008, the frequency of collapses and landslides in the region has increased rapidly, along with a greater frequency of debris flows. As a result of these debris flows, the villages, farms, and infrastructure in the study area have been seriously impacted.

## Methods

### SCS-CN hydrological model

The SCS-CN method considers underlying surface characteristics of the watershed, such as soil, vegetation, slope, and land use. It can account for the indirect influence of human activities, establish the relationship between hydrological model parameters and remote sensing

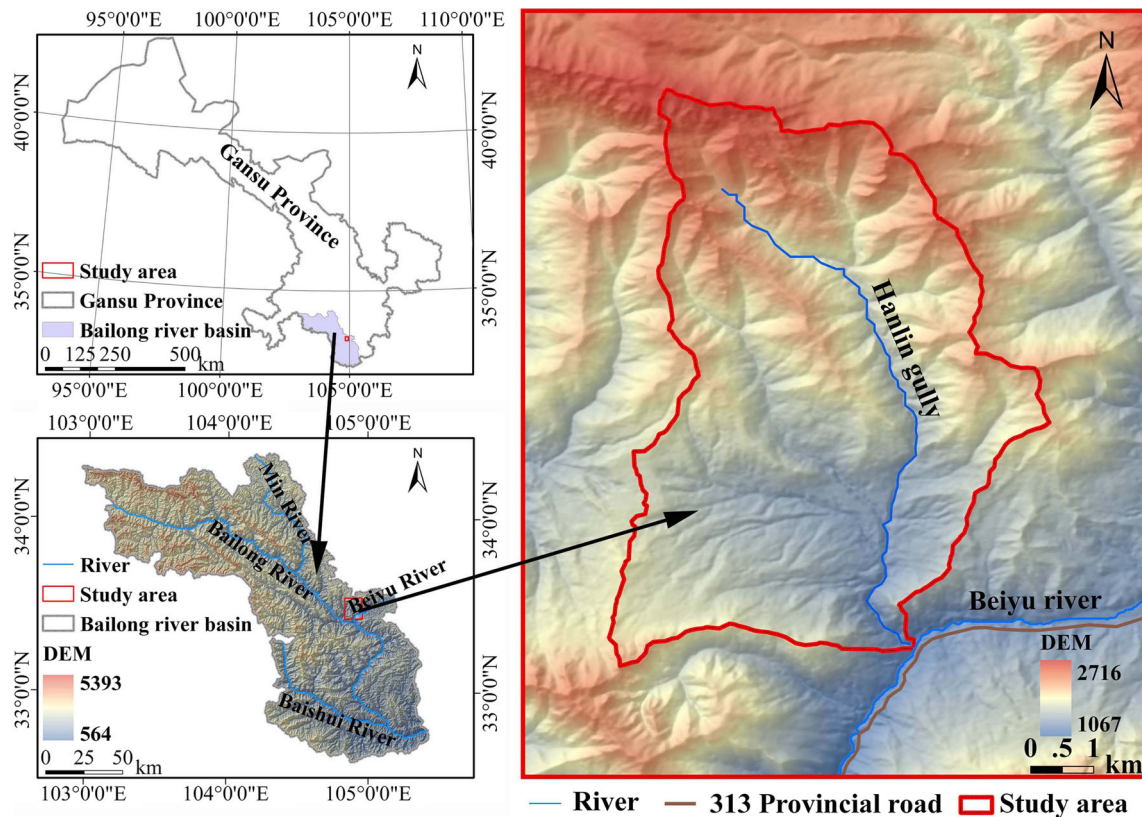


**Fig. 1** Study area

information, and be used to the estimate runoff with no direct data. Direct runoff  $Q$  (mm) is expressed as (Williams and LaSeur 1976; Rawls et al. 1992; Bhuyan et al. 2003; Mishra and Singh 2003):

$$Q = \begin{cases} \frac{(P - 0.2S)^2}{(P + 0.8S)} & P \geq 0.2S, \\ 0 & P < 0.2S, \end{cases} \quad (1)$$

where  $P$  (mm) is the total rainfall and  $S$  (mm) is the potential maximum infiltration.

Equation (1) shows that runoff depends on  $P$  and  $S$  before rainfall;  $S$  is related to soil texture, land use, and AMCs. Because of the range of variation of  $S$  and to facilitate data acquisition,  $S$  is derived from a mapping equation expressed in terms of the CN:

$$S = \frac{25,400}{CN} - 254, \quad (2)$$

where CN, an empirical dimensionless parameter, indicates the runoff-producing potential of a watershed and is dependent on factors such as soil AMC, slope, land use, and soil texture. As can be seen from Eq. (2), a high CN value indicates higher runoff and lower infiltration and a

low CN value indicates lower runoff and higher infiltration. Because of the difficulty of obtaining soil parameters in this area, the soil parameters were obtained by matching them to similar soil descriptions found in USDA (2012). Other parameters were obtained through testing during the study.

The basin was divided into geomorphic subunits prior to calculating the runoff of the watershed. Using the digital elevation model (DEM; spatial resolution of 12.5 m) and the hydrological analysis tool of ArcGIS v.9.3, a digital drainage network was generated to recognize the main stream and tributaries of the study area.

Incorporating remote sensing and land-use and soil-type maps of the study area, ArcGIS was used to calculate the area of each land use and soil type in each sub-basin. Combining the AMCs and the table of CN values from the SCS-CN model, the average CN value of each sub-basin was determined using an area-weighted method. The CN value of every specific land use, the soil hydrologic group (HYDGRP), and the precipitation at different times were input as attribute values. The runoff depth and volume of each sub-basin was then calculated using the SCS-CN model.

## FLO-2D debris flow model

The FLO-2D software (v.12.11.02) simulates 2D mudflow or debris flow to determine the average velocity in the  $x$ -axis direction (downstream), average velocity in the  $y$ -axis direction (side to side), and flow depth. The governing continuity and momentum equations (O'Brien et al. 1993; O'Brien 2006) are shown below:

### Continuity equation

$$\frac{\partial h}{\partial t} + \frac{\partial hV_x}{\partial x} + \frac{\partial hV_y}{\partial y} = i. \quad (3)$$

### Momentum equations

$$S_{fx} = S_{bx} - \frac{\partial h}{\partial x} - \frac{V_x}{g} \left( \frac{\partial V_x}{\partial x} \right) - \frac{V_y}{g} \left( \frac{\partial V_x}{\partial y} \right) - \frac{1}{g} \left( \frac{\partial V_x}{\partial t} \right), \quad (4)$$

$$S_{fy} = S_{by} - \frac{\partial h}{\partial y} - \frac{V_y}{g} \left( \frac{\partial V_y}{\partial y} \right) - \frac{V_x}{g} \left( \frac{\partial V_y}{\partial x} \right) - \frac{1}{g} \left( \frac{\partial V_y}{\partial t} \right), \quad (5)$$

where  $h$  (m) is mudflow or debris flow depth,  $i$  (mm/h) is rainfall intensity,  $t$  (h) is time,  $g$  ( $\text{m/s}^2$ ) is acceleration of gravity,  $V_x$  (m/s) and  $V_y$  (m/s) are average velocities of the  $x$ - and  $y$ -axis directions, respectively,  $S_{bx}$  and  $S_{by}$  are the bed slopes of the  $x$ - and  $y$ -axis directions, respectively, and  $S_{fx}$  and  $S_{fy}$  are the friction slopes of the  $x$ - and  $y$ -axis directions, respectively.

The 3-year maximum rainfall intensity value for the study area and equivalent Manning coefficients ( $n$ ) from the U.S. Army HEC-1 manual (Warwick et al. 1991) were used for input to the model. The debris bulk density value ( $G_S$ ) was derived from debris flow deposits. The laminar retardation coefficient ( $K$ ) was set using the work of Woolhiser (1975) combined with field investigation results and the yield stress ( $\tau_y$ ) and coefficient of viscosity ( $\eta$ ) were determined using historical natural disasters in the study area.

First, a digital terrain model (DTM) was overlain with a grid system. The grid developer system (GDS) processor module of the FLO-2D program generates a grid system on a DTM database and assigns elevations to the grid elements. FLO-2D can be used to generate a flood hydrograph at a specific location by modeling the rainfall–runoff in the upstream watershed. The specific simulation steps were as follows: open the GDS program, import terrain elevation data, create the grid, import aerial images, outline the project area boundaries computational domain, interpolate the digital terrain elevation data and assign the grid element elevations, assign hydrographs to select inflow element, select outflow grid elements, and run the FLO-2D model. A flow chart of the debris flow simulation is shown on Fig. 2.

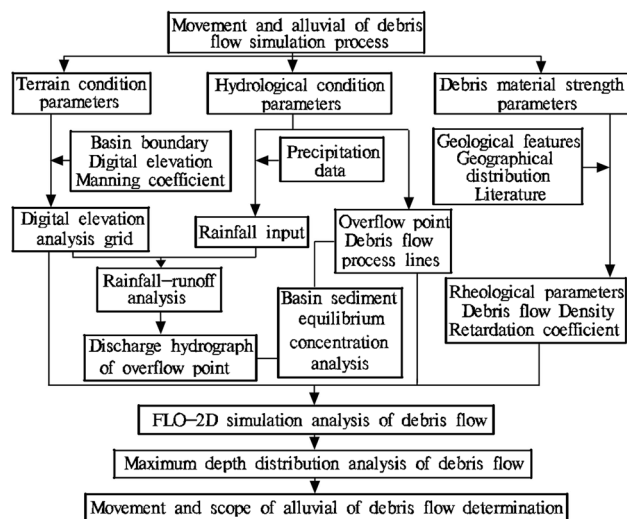


**Fig. 2** Flowchart of simulation process for debris flow movement

## Results and discussion

### Hydrological simulation

Using the SCS-CN model and based on the total precipitation 5 days prior to the event, the moisture content of the study area soil was classified as dry (AMC I), average (AMC II), and moist (AMC III; Table 1) (Azoozr and Arshad 1996; Tomlinson 2003). The soil was divided into four types—A, B, C, and D (Table 2)—based on minimum infiltration rates according to Dokuchaev (2000).

Remote sensing images were used to identify the main land uses in the study area as grazing, forest, crop, and

**Table 1** Antecedent moisture conditions (AMC) in the study area

Soil moisture classification (SCS-CN)	Precipitation of previous 5 days (mm)	
	Crop growth stage	Crop dormancy stage
AMC I	<30	<15
AMC II	30–50	15–30
AMC III	>50	>30

**Table 2** Hydrologic soil indicators

Soil groups	Minimum infiltration rate (mm/h)	Typical soil characteristics
A	>7.26	Sand, sandy loam, loam sand
B	3.81–7.26	Loam, silt loam
C	1.27–3.81	Sandy clay loam
D	0.00–1.27	Clay loam, silt clay loam, sand clay, silt clay, clay

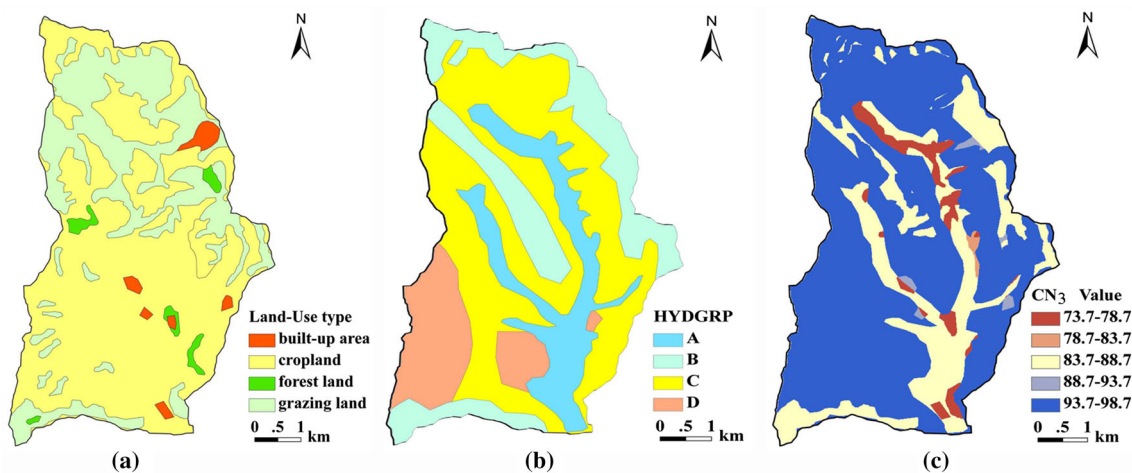


**Fig. 3** Land uses, soil hydrologic group, and CN3 values in study area

**Table 3** Soil hydrologic groups in the study area

Study area soils	Hydrologic soil groups
Gravel soil	A
Loam	B
Silt clay	C
Silty soil	B
Paddy soil	D
Silt clay loam	D

**Table 4** CN<sub>2</sub> values in AMC II conditions for the study area

	CN <sub>2</sub> value for different soil hydrologic groups			
	A	B	C	D
Grazing	55	55	77	77
Forest	49	69	84	84
Cropland	76	85	94	94
Built-up area	57	72	81	96

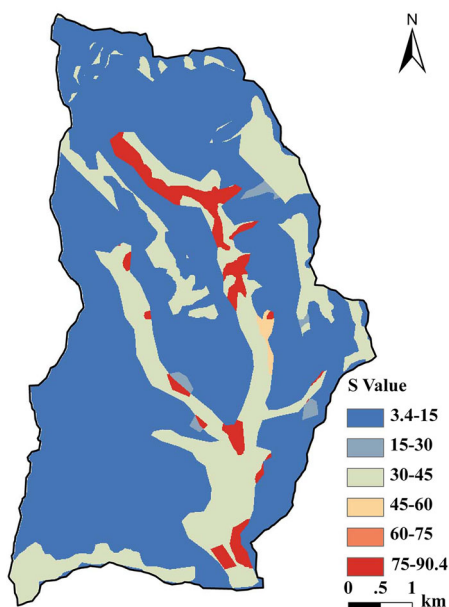


**Fig. 4** Distribution of S value in study area

built-up areas (Fig. 3a). Soil in the watershed is mainly gravel soil, loam, silty clay, clay, and paddy soil. The corresponding soil HYDGRPs of the different types of soil in the study area are shown in Table 3 and Fig. 3b. Using the standard CN values from the SCS model, a CN<sub>2</sub> value for various soil types was determined under AMC II soil moisture conditions, as previously done by Tomlinson (2003) and USDA (2012) (Table 4).

Based on land uses, soil HYDGRP features, and AMCs during the testing period, CN values were calculated for AMC I and AMC III soil moisture conditions that corresponded with CN<sub>1</sub> and CN<sub>3</sub>. CN<sub>2</sub> values under AMC II soil moisture conditions were calculated based on Table 5 and Eqs. (6) and (7). The values of CN<sub>3</sub> are shown in Table 5 and the distribution of CN<sub>3</sub> is shown on Fig. 3c.

$$CN_1 = 4.2CN_2 / (10 - 0.058CN_2), \tag{6}$$

$$CN_3 = 23CN_2 / (10 + 0.13CN_2). \tag{7}$$

A 10–15-day precipitation time interval (the time between the precipitation events) was used to reduce the influence of antecedent rainfall on soil moisture. Light, moderate, and heavy precipitation events in the Wudu district on 1 July 2005 (4.6 mm), 18 July 2005 (10.4 mm),

**Table 5** CN<sub>3</sub> values in AMC III conditions for the study area

Land uses	CN <sub>3</sub> value for different soil hydrologic groups			
	A	B	C	D
Grazing	74	74	89	89
Forest	69	84	92	92
Cropland	88	93	97	97
Built-up area	75	86	91	98

and 31 July 2005 (25.4 mm), along with the historical maximum precipitation of 41 mm/h, were selected. Although the light precipitation event would not generate a debris flow, all events were used to simulate the different hydrological processes.

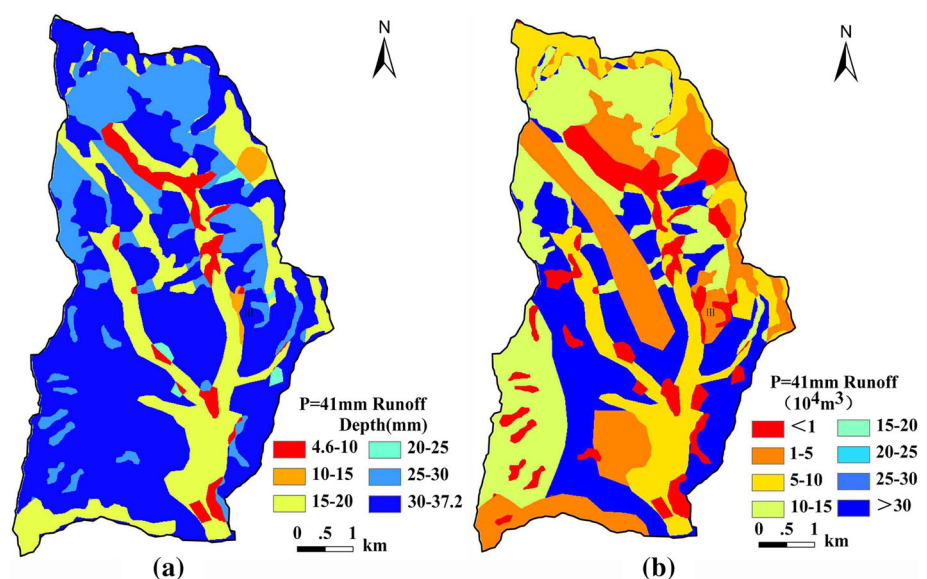
A CN<sub>3</sub> value distribution chart of the study area was drawn for the 1 July precipitation event using ArcGIS and the selected precipitation data (Fig. 3c). The *S* distribution chart (Fig. 4) in the watershed was calculated based on the flow generation conditions and Eq. (2) in the SCS model. Using GIS, a map was created that included land use types and soil HYDGRPs. After inputting the CN values of the different land uses and soil HYDGRPs selected into the property table of the generated map, the runoff depths and runoff volumes were calculated in the study area at different time intervals by Eq. (1). For the soils in the same HYDGRP, different land uses were shown to exhibit different run-off patterns. Forest land had the highest runoff retention followed by grazing land, built-up areas, and crop land. Within a similar land use, such as low-level grassland, different soil environments generated different run-off depths. Paddy soil generated the highest run-off depth followed by silty clay, silty clay loam, silt, loam, and

gravel soil. The higher the CN value, the greater the runoff, which indicates that most precipitation would be converted into runoff in the sub-branches.

Based on the *S* value in Fig. 4, the sub-basin runoff was calculated according to Eq. (1); the accumulated total runoff volumes were approximately 33949, 139071, and 516112 m<sup>3</sup> when the precipitation was 4.6, 10.4, and 25.4 mm, respectively. The total runoff was approximately 970,062 m<sup>3</sup> when the maximum hourly precipitation was 41 mm. Distribution diagrams for the runoff depth and runoff volume are shown in Fig. 5a, b for a total precipitation of 41 mm. Through numerical simulation, the amounts of runoff would be lower when the precipitation was lower, such as when the precipitation event was 4.6 mm. Moreover, when the *P* of the sub-watershed was less than 0.2*S*, no runoff would be generated and all the precipitation would be transferred into infiltration. In contrast, the runoff depth would be higher when the precipitation was higher, such as when the precipitation 25.4 mm. Runoff would be generated in all of the study area when the *P* of the sub-branch watershed was greater than 0.2*S*, which demonstrates the close relationship with the land use and texture of the soil.

To test the accuracy of the runoff simulation, two precipitation stations were established on the upstream and downstream hydraulic stations in the channel gate of the study area. On 20 July 2012, precipitation of 10.6 mm occurred. The measured stream flow of the upstream and downstream hydraulic stations was 7.15 and 7.29 million m<sup>3</sup>, respectively. The difference in the two flows was about 0.14 million m<sup>3</sup>, essentially the runoff from the study area. This was consistent with the simulated runoff volumes of 0.14 million m<sup>3</sup> when the *P* was 10.4 mm on 18 July 2005

**Fig. 5** Distribution of simulated runoff depth (a) and simulated runoff volume (b) for a 41 mm rainfall



and confirmed the reliability of the SCS model for simulating the hydraulic process.

### Simulation of debris flow

Based on the geographic and geomorphic conditions of the study area and the occurrences of debris flows in the Wudu district in recent years (most of the debris flows occurred between July and September), field investigations and sampling were performed in the Hanlin gully during the middle 10 days of July 2012 (flood season). The average grain classification curve is shown in Fig. 6. A relatively accurate bulk density value ( $G_S$ ) for material proportions of the debris flow channel was obtained using grain size analyses.

Wudu district records indicate that the study area has experienced relatively large-scale debris flows in the past 5 years. Recent precipitation peaked in southern Gansu City from July to September in 2010 and resulted in debris flow in several debris flow channels. The heavy rainstorm of 12 August 2010 in southern Gansu resulted in large debris flows and the study area experienced significant, associated damage. Accordingly, the results of the large debris flow in the Hanlin gully that occurred on 12 August 2010 were used for parameter calibration. The landform model was the 12.5-m resolution DEM in the study area; the maximum precipitation was 41 mm/h; the bulk density of the debris flow was 2.25 g/cm<sup>3</sup>; and the retardation factor of the flow layer was 2,285. The parameter calibrations for yield stress and coefficient of viscosity were 1,200 Pa and 10 Pa s, respectively. Manning coefficient values were 0.05/0.15/0.25/0.3/0.4. The simulation of the debris flow was performed using FLO-2D PRO (v. 12.11.02), which incorporates the FLO-2D model and includes the RAIN and MUDFLO-2D modules. The basic inflow element and a hydrograph of the FLO-2D model for

simulating the movement of debris flow are shown in Fig. 7 (O'Brien 2006).

The channel section was calculated for modeling of the middle and lower streams of the study area and included several small sub-channels. The total length of the modeled watershed was 9.45 km. The DEM of the study area was divided into 10 × 10 m grids resulting in 263,525 grids.

The parameter conditions and parameter calibrations were input into the FLO-2D model to simulate the movement and deposition processes in the debris flow channel. The simulated velocity and impact force of the debris flow are shown in Fig. 8a, b. The final depth of deposition of the debris flow in the channel is shown in Fig. 8c. The maximum flow velocity of the simulated debris flow was 23.1 m/s, the maximum impact force was 253 × 10<sup>4</sup> kN, and the maximum deposit depth flow was 27.9 m from the Hanlin gully to Beiyu River. Note that although the maximum flow velocity of 23.1 m/s is high, it is linked to how the FLO-2D PRO software works. The simulation begins using water as the first boot mode and mixes it with sediment to form the debris flow. The maximum velocity refers to the process of the water and sediment forming the debris flow.

Figure 8a shows that the highest velocity of debris flow was in the middle reach of the channel and that the velocity gradually decreases after reaching the lower stream. The result was consistent with the process of energy storage, startup, and energy consumption of physical movement. The distribution of the impacting power is shown in Fig. 8b. The impacting power of the debris flow movement reached its highest value at the intersection of branches and was lowest at the entrance to Beiyu River. When the velocity of the debris flow was relatively high, deposition was low. When the velocity and impacting power decreased from the lower stream to the outlet, gradual deposition began, reaching a maximum depth at the outlet

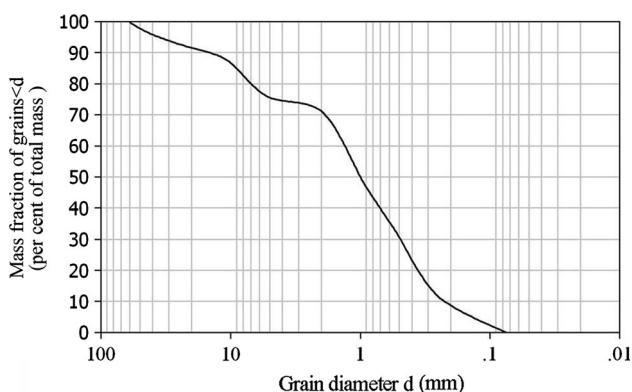


**Fig. 6** Grain size analysis of soil in study area

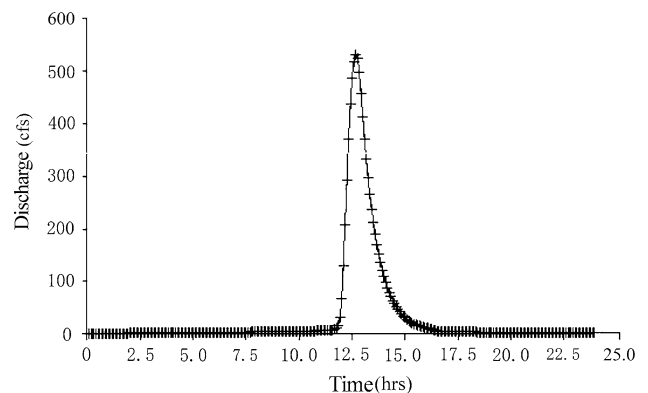


**Fig. 7** Unit hydrograph of discharge generated from the FLO-2D rainfall-runoff module

**Fig. 8** Simulated results of debris flow in study area: **a** velocity, **b** impact force, **c** deposition depth, and **d** comparison of actual hazard zone to simulated hazard zone

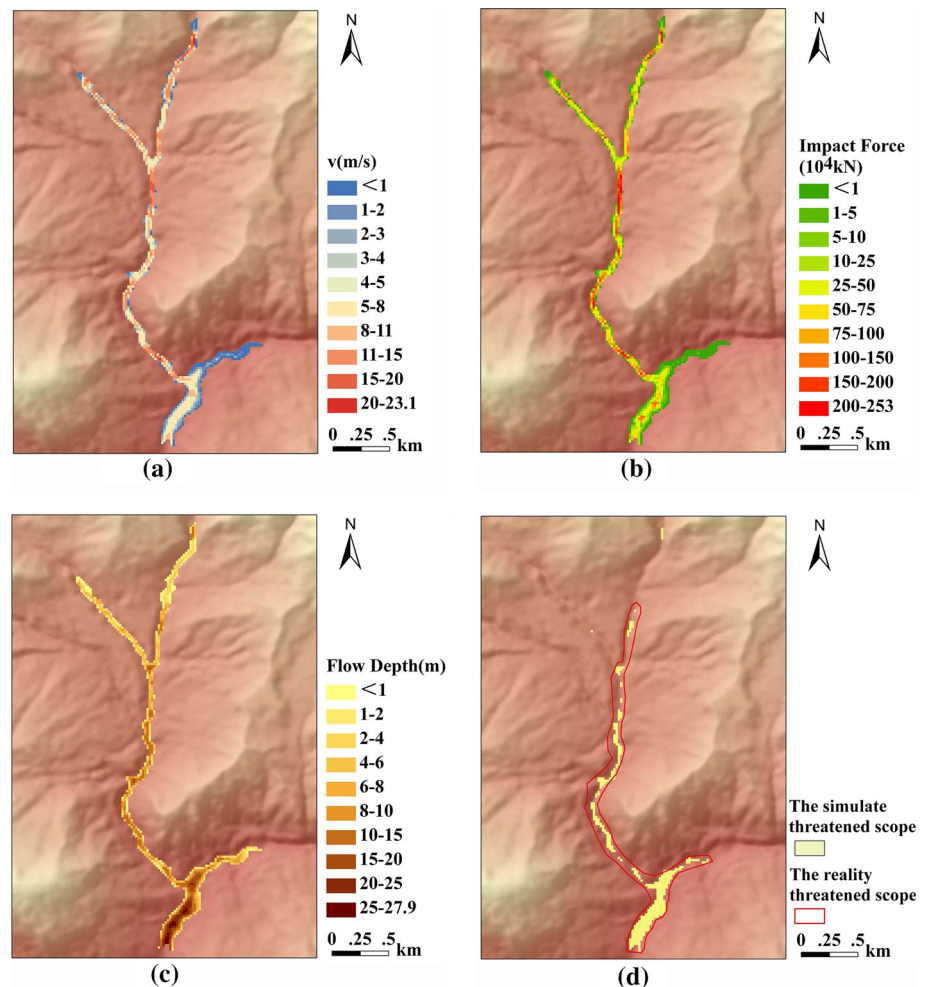


(Fig. 8c), which corresponds well with the deposition process of the actual debris flow. The results showed the maximum depth of deposition along the cross section from the upper stream to the outlet reached 6 m (Fig. 8). Destructive damage would be caused to villages, farms, and infrastructure located at the lower stream and outlet of the gully when the maximum deposition depth is between 10 and 13 m over an area of about 0.414 km<sup>2</sup>.

The simulation results of the area under threat are shown in the yellow area in Fig. 8d, with the actual area impacted by the August 12th event in southern Gansu outlined in red. The actual hazard zone was determined by field investigations and by means of a 2011 questionnaire for residents (Fig. 8d).

Human-influenced land uses (farming land on hills and grasslands) and soils with relatively high infiltration rates (gravel soil, loamy soil) both demonstrated a greater capacity to store and retain water. Because the upstream sub-branch watersheds are more susceptible to soil instability and associated geological disasters, such as small regional landslides and collapses, these areas provide material sources for the occurrence of debris flows.

The FLO-2D model simulation of the debris flow deposition process demonstrated that the maximum flow velocity decreases when the solids concentration of the debris flow is higher than 50 %. Results over several simulations were consistent with actual measurements. Thus, volume concentration plays a critical role in the accuracy of simulation results. The simulation results for the deposition process of debris flows using the FLO-2D model were consistent with the actual measured results (Fig. 8d).

## Conclusion

The FLO-2D PRO model was used to simulate the movement and deposition processes of debris flow. The application of the SCS-CN model in an ArcGIS environment increased the efficiency of the calculations in the debris flow simulation. Total runoff volumes were calculated to be about  $3.39 \times 10^4$ ,  $13.9 \times 10^4$ , and  $51.6 \times 10^4$  m<sup>3</sup> when the precipitation was 4.6, 10.4, and 25.4 mm, respectively.



The total runoff volume was about  $97 \times 10^4 \text{ m}^3$  when the maximum hourly precipitation was 41 mm.

FLO-2D PRO effectively simulated the movement and deposition processes of the debris flow and was consistent with the actual measurements from that debris flow. The simulation of Hanlin gully debris flow demonstrates that the maximum flowing velocity was 23.1 m/s, the maximum impacting power was  $253 \times 10^4 \text{ kN}$ , the maximum movement and depositing depth was 27.9 m, and the hazard zone was about  $0.414 \text{ km}^2$ . The FLO-2D model was applied to the debris flow that resulted from the storm of 12 August 2010 in southern Gansu to simulate the movement and depositional process of debris flow. The hazard area of the debris flow calculated from the simulation analysis was consistent with the actual measured hazard area of that debris flow. The simulation results proved the effectiveness and practicality of the FLO-2D PRO model. The model effectively simulated the movement and depositional process of the debris flow. Further research on the infiltration depth, runoff depth, and runoff of the branch watersheds of the debris flow channel could refine understanding of the processes and help predict debris flow disasters.

The performance of the simulation was mainly demonstrated by the functions like effective data treatment, spatial analysis, model calculation, and visualization analysis.

Verification demonstrated that these results were usable and could provide a reliable, scientific basis for the prediction of the occurrence of disaster-causing debris flows, thus providing a basis for the protection of the lives, property, and economy of the local population.

**Acknowledgments** The paper was supported by the National Key Technology R&D Program (No. 2011BAK12B05). We wish to thank Academician Zuyu Chen and Prof. Xingmin Meng for their constructive suggestions to prepare the manuscript. We also thank Dr. Limin Tian, Shi Qi and Na Ning for the field works and laboratory analysis. We appreciate the contributions of three anonymous reviewers and Dr. Igwe Ogbonnaya, all of whom contributed to improve the manuscript.

**References**

Aleotti P, Polloni G (2003) Two-dimensional model of the 1998 Sarno debris flows (Italy): preliminary results. In: Rickenmann D, Chen CL (eds) Third international conference on debris-flow hazards mitigation: mechanics, prediction and assessment. Mill Press, Rotterdam, pp 553–563

Azoozr H, Arshad MA (1996) Soil infiltration and hydraulic conductivity under long-term no-tillage and conventional tillage systems. *Can J Soil Sci* 76:143–152

Bai SB, Wang J, Zhang FY, Pozdnoukhov A, Kanevski M (2008) Prediction of landslide susceptibility using logistic regression: a case study in Bailongjiang River Basin, China. In: Ma J, Yin Y, Yu J, Zhou SG (eds) Proceedings of the fifth international conference on fuzzy systems and knowledge discovery (FSKD 2008), vol 4. IEEE, Los Alamitos, pp 647–651

Bertolo P, Wieczorek GF (2005) Calibration of numerical models for small debris flows in Yosemite Valley, California, USA. *Nat Hazards Earth Syst Sci* 5:993–1001

Bhuyan SJ, Mankin KR, Koelliker JK (2003) Watershed-scale AMC selection for hydrologic modeling. *Trans ASABE* 46(2):303–310

Chen SC, Wu CY, Huang BT (2010) The efficiency of a risk reduction program for debris-flow disasters—a case study of the Songhe community in Taiwan. *Nat Hazards Earth Syst Sci* 10(7):1591–1603

Dai FC, Lee CF (2001) Frequency–volume relation and prediction of rainfall-induced landslides. *Eng Geol* 59:253–266

Doglioni A, Simeone V (2014) Geomorphometric analysis based on discrete wavelet transform. *Environ Earth Sci* 71(7):3095–3108

Dokuchaev VV (2000) Russia soil classification. *Soil Sci Inst Russ Acad Agric Sci* 20:1–232

Dongqian Z, Jining C, Haozheng W, Qingyuan T, Shangbing C, Zheng S (2009) GIS-based urban rainfall–runoff modeling using an automatic catchment-discretization approach: a case study in Macau. *Environ Earth Sci* 59(2):465–472

Garcia R, López JL, Noya M, Bello ME, Bello MT, Gonzalez N, Paredes G, Vivas MI, O’Brien JS (2003) Hazard mapping for debris flow events in the alluvial fans of northern Venezuela. In: Rickenmann D, Chen CL (eds) Third international conference on debris-flow hazards mitigation: mechanics, prediction and assessment. Mill Press, Rotterdam, pp 10–12

Gupta P, Punalekar S, Panigrahy S, Sonakia A, Parihar J (2012) Runoff modeling in an agro-forested watershed using remote sensing and GIS. *J Hydrol Eng* 17(11):1255–1267

Hadadin N (2013) Evaluation of several techniques for estimating stormwater runoff in arid watersheds. *Environ Earth Sci* 69(5):1773–1782

Hsu SM, Chiou LB, Lin GF, Chao CH, Wen HY, Ku CY (2010) Applications of simulation technique on debris-flow hazard zone delineation: a case study in Hualien County, Taiwan. *Nat Hazards Earth Syst Sci* 10:535–545

Jain M, Durbude D, Mishra S (2012) Improved CN-based long-term hydrologic simulation model. *J Hydrol Eng* 17(11):1204–1220

Jena S, Tiwari K, Pandey A, Mishra S (2012) RS and geographical information system-based evaluation of distributed and composite curve number techniques. *J Hydrol Eng* 17(11):1278–1286

Mishra SK, Singh VP (2003) Soil Conservation Service curve number (SCS-CN) methodology. Kluwer Academic Publishers, Dordrecht, pp 43–47

Mishra SK, Pandey A, Singh VP (2012) Special issue on Soil Conservation Service curve number (SCS-CN) methodology. *J Hydrol Eng* 17(11):1157

Nagarajan N, Poongothai S (2012) Spatial mapping of runoff from a watershed using SCS-CN method with remote sensing and GIS. *J Hydrol Eng* 17(11):1268–1277

National Soil Survey Office (NSSO) (1998) Soil of China. China Agriculture Press, Beijing, pp 20–29

O’Brien JS (2006) FLO-2D user’s manual, version 2006.01. FLO-2D Software, Inc., Nutrioso

O’Brien JS, Julien PJ, Fullerton WT (1993) Two-dimensional water flood and mudflow simulation. *J Hydraul Eng* 119(2):244–261

Peng SH, Lu SC (2012) FLO-2D simulation of mudflow caused by large landslide due to extremely heavy rainfall in southeastern Taiwan during Typhoon Morakot. *J Mt Sci* 10(2):207–218

Rawls WJ, Ahuja LR, Brakensiek DL, Shirmohammadi A (1992) Chapter 5: infiltration and soil water movement. In: Maidment DR (ed) Handbook of hydrology. McGraw-Hill, Inc., New York, pp 1–46

Sahu RK, Mishra SK, Eldho T (2012) Improved storm duration and antecedent moisture condition coupled SCS-CN concept-based model. *J Hydrol Eng* 17(11):1173–1179

- Suresh Badu P, Mishra SK (2012) Improved SCS-CN-inspired model. *J Hydrol Eng* 17(11):1164–1172
- Takahashi T (2007) Debris flow: mechanics, prediction and countermeasures. Taylor and Francis Group, London. ISBN 978-0-415-43552-9
- Tomlinson P (2003) Review: strategic environmental assessment in transport and land use planning. *Environ Impact Assess Rev* 23:133–136
- Tsai TL, Wang JK (2011) Examination of influences of rainfall patterns on shallow landslides due to dissipation of matric suction. *Environ Earth Sci* 63(1):65–75
- Turconi L, De SK, Demurtas F, Demurtas L, Pendugiu B, Tropeano D, Savio G (2013) An analysis of debris-flow events in the Sardinia Island (Thyrrhenian Sea, Italy). *Environ Earth Sci* 69(5):1931–1938
- United States Department of Agriculture, USDA (2012) Part 630 hydrology—national engineering handbook. United States Department of Agriculture, Natural Resources Conservation Service. <http://directives.sc.egov.usda.gov/viewerFS.aspx?hid=21422>
- Warwick JJ, Haness SJ, Dickey RO (1991) Integration of an ARC/INFO GIS with HEC-1. In: Anderson JL (ed) Water resources planning and management and urban water resources, proceedings of the 18th conference. ASCE, New York, pp 1029–1033
- Williams JR, LaSeur WV (1976) Water yield model using SCS curve numbers. *J Hydraul Div* 102(9):1221–1253
- Williams J, Kannan N, Wang X, Santhi C, Arnold J (2012) Evolution of the SCS runoff curve number method and its application to continuous runoff simulation. *J Hydrol Eng* 17(11):1221–1229
- Woolhiser DA (1975) Simulation of unsteady overland flow. In: Mahmood K, Yevjevich V (eds) Unsteady flow in open channels. Water Resources Publications, Fort Collins, pp 485–508
- Wu YH, Liu KF, Chen YC (2012) Comparison between FLO-2D and Debris-2D on the application of assessment of granular debris flow hazards with case study. *J Mt Sci* 10(2):293–304
- Xu FG, Yang XG, Zhou JW (2014) An empirical approach for evaluation of the potential of debris flow occurrence in mountainous areas. *Environ Earth Sci* 71(7):2979–2988
- Youn C, Pandit A (2012) Estimation of average annual removal efficiencies of wet detention ponds using continuous simulation. *J Hydrol Eng* 17(11):1230–1239
- Yu BF (2012) Validation of SCS method for runoff estimation. *J Hydrol Eng* 17(11):1158–1163
- Zhang P, Ma J, Shu H, Wang G (2014) Numerical simulation of erosion and deposition debris flow based on FLO-2D Model. *J Lanzhou Univ (Nat Sci)* 50(3):363–368 (in Chinese)
- Zhuang JQ, Cui P, Peng JB, Hu KH, Iqbal J (2013) Initiation process of debris flows on different slopes due to surface flow and trigger-specific strategies for mitigating post-earthquake in old Beichuan County, China. *Environ Earth Sci* 68(5):1391–1403